Engineering different B doping modes on Ru active sites for efficient alkaline hydrogen evolution

Xuzhuo Sun,[a] Cancan Cao,[a] Yuying Fu,[a] Jing Chen, [a] Bo Li,*[a] Liuqing Fan,[a] Jing Yang,*[c] and Haibo Zhang*[b]

[a] College of Chemistry and Chemical Engineering, Henan University of Technology, Zhengzhou 450001 (China)

[b] College of Chemistry and Molecular Sciences, National Demonstration Center for Experimental Chemistry, Wuhan University, Wuhan 430072 (China)

[c] College of Health Science and Environmental Engineering, Shenzhen Technology University, Shenzhen 518118 (China)

*Corresponding author. E-mail address: haut-libo@haut.edu.cn (Prof. B. Li), yangjing2@sztu.edu.cn (Dr. J. Yang); haibozhang1980@gmail.com (Prof. H. Zhang)

Table of Contents

Experimental section

Chemicals and materials

The hydroxylated multi-walled carbon nanotubes (length 0.5-2 μm, 95%) was purchased from Nanjing XFNANO Materials Tech Co., Ltd. $Cs_2[B_{12}H_{12}]$ (AR 98%), $RuCl_3$ xH_2O (AR, 35-42%) were purchased from Aladdin Co., Ltd. Nafion perfluorinated resin solution (5 wt %) was purchased from Sigma-Aldrich corporation. Pt/C (Pt: 20 wt %) was purchased from Alfa Aesar. Carbon paper (HCP010N) was purchased from Shanghai Hesen Electrical Co., Ltd. Ultrapure water with a resistivity of 18.25 MΩ cm was used in whole experimental process. All chemicals were of analytical grade and used without further purification.

Methods

Synthesis of *closo*-$[B_{12}H_{12}]^{2-}$/OH^{2+}-CNT

OH-CNT (60 mg) was well dispersed in 30 ml of 0.1 M HCl (pH=1) solution and continuously ultrasonicated for 30 min. Subsequently, Cs_2[*closo*-$B_{12}H_{12}$] was added to the suspension solution, sonicated for 30 min, and then magnetically stirred for another 2 h. After the solution was filtered, washed three times with water and ethanol, then dried at 60 °C for 12 h.

Synthesis of Ru/B-CNT

Closo-$[B_{12}H_{12}]^{2-}$/OH^{2+}-CNT (30 mg) was well dispersed in 30 ml of aqueous solution and continuously ultrasonicated for 30 min. After N_2 purged for 30 minutes, $RuCl_3$ xH_2O (15 mg) was added to the suspension solution, and magnetically stirred for 2 h. Then the solution was filtered, washed three times with DI water and one time with

ethanol, and dried at 60 °C for 12 h. The sample was denoted as **B-Ru/CNT**. The B-Ru/CNT was calcined at 600 °C for 2 h under N_2 atmosphere with the heating rate of 10 °C/min and the Ru/B-CNT was obtained.

Synthesis of Ru/CNT

OH-CNT (60 mg) was well dispersed in 30 ml water solution and continuously ultrasonicated for 30 min. Subsequently, $RuCl_3$ xH_2O (15 mg) was added to the suspension solution, and magnetically stirred for 2 h. After the solution was filtered, washed three times with water and one times with ethanol, and dried at 60 °C for 12 h. The obtained powder was calcined at 600 °C for 2 h under N_2 atmosphere with the heating rate of 10 °C/min.

Synthesis of Ru/CNT-Na

Ru/CNT-Na was prepared in similar procedure except that $NaBH_4$ is used as a reductant in a same molar amount as *closo*-$[B_{12}H_{12}]^{2-}$.

Prepare the working electrode

To prepare the working electrode, each catalyst (3 mg) was dispersed into 0.72 ml solution composed of 5:1 =ethanol: 5 wt% Nafion solution) and then the uniform catalyst ink was preparation by sonication (200 W, 2 h). Then, the 60 μl catalyst ink was dropped on the surface of the carbon paper (area: 0.25 cm^2) with a loading of 1 mg cm^{-2}.

Electrochemical measurements

The electrochemical analysis was performed at the CHI660E electrochemical workstation with a standard three-electrode configuration. Before all the tests, the

reference electrode was experimentally calibrated against reversible hydrogen electrode (RHE) in H_2-saturated electrolyte, respectively. The Ru/B-CNT, B-Ru/CNT, and Ru/CNT catalysts directly served as a working electrode, together with a Graphite rod counter electrode and a reference electrode (Hg/HgO for HER). All the experiment was tested in 1 M KOH. The linear sweep voltammetry (LSV) polarization curves were measured with a scan rate of 5 mV s^{-1}, and before the measurement, the catalyst was activated by 20 cycles of cyclic voltammetry (CV) test until reaching a relatively steady state. The potential range was -0.4 V~ 0.3 V vs. RHE for HER. All polarization curves were corrected by *i*R.

$$E \text{ (vs. RHE)} = E \text{ (vs. Hg/HgO)} + 0.059\text{pH} + 0.098 - 0.9\ i\text{R}.$$

Tafel curves can be derived from LSV curves using the equation of $\eta = a + b \log j$, where η refers to the overpotential, b is the Tafel slope and a denotes the intercept.

The electrochemical impedance spectroscopy (EIS) was performed under the frequency range at 10^{-2}~10^{5} Hz with an amplitude of 5 mV. Nyquist curve and Bode plots were obtained from the impedance data. The double-layer capacitance (C_{dl}) was used to estimate the electrochemically active surface area (ECSA). The cycling voltammetry (CV) measurements were conducted in the non-Faradic region with scanning rates of 10, 20, 30, 40, 50 mV s^{-1} to investigate the double-layer capacitor. The C_{dl} values were then calculated by measuring the slope of the fitting lines of half of the current density difference.

Chronoamperometric curves operated at a fixed voltage corresponding to 10 mA cm^{-2}. The accelerated durability test of the catalyst was conducted by continuously

CV measurement between 0.1 V~ -0.2 V (vs. RHE) for 10, 000 cycles at a scan rate of 100 mV s^{-1}, and the polarization curves before and after CV measurement were recorded.

Characterization

The crystal structures of the samples were characterized by a Bruker D8 Advance Powder X-ray diffractometer with Cu Kα radiation source (λ=1.54 Å). The size and shape of the as-prepared samples were analyzed by transmission electron microscopy (TEM) and high-resolution transmission electron microscopy (HR-TEM, Talos F200X). The instrument also recorded HAADF-STEM images and corresponding atomic-resolution EDX element mapping. X-ray photoelectron spectroscopy (XPS) was recorded on a PHI5000VersaProbell using Al Kα X-ray source to analyse the elements binding states. The contents of Ru and B were obtained by inductively coupled plasma-optical emission spectrometer (ICP-OES) (Aglient 5110).

DFT Calculation Method

To get further insight into the effects of B atoms on the HER performance, DFT calculations are utilized to understand the underlying mechanism of the HER process. The Vienna Ab initio Simulation Package (VASP) [1,2] was performed all density functional theory (DFT) calculations within the generalized gradient approximation (GGA) using the Perdew-Burke-Ernzerhof (PBE) [3] formulation. The projected augmented wave (PAW) potentials [4,5] were chosen to describe the ionic cores and

take valence electrons into account using a plane wave basis set with a kinetic energy cutoff of 450 eV. Partial occupancies of the Kohn−Sham orbitals were allowed using the Gaussian smearing method and a width of 0.05 eV. For the optimization of both geometry and lattice size, the Brillouin zone integration was performed with a 0.04 $Å^{-1}$ *k*-mesh Monkhorst-Pack sampling [6]. The self-consistent calculations applied a convergence energy threshold of 10^{-5} eV. The equilibrium geometries and lattice constants were optimized with maximum stress on each atom within 0.02 eV $Å^{-1}$. The 17 Å vacuum layer was normally added to the surface to eliminate the artificial interactions between periodic images. The weak interaction was described by DFT+D3 method using empirical correction in Grimme's scheme [7, 8]. Spin polarization method was adopted to describe the magnetic system. Isosurface level of charge density difference was set at 0.002 eV $Å^{-3}$.

The adsorption energy was calculated as: E_{ads} = E(*adsorbent) - E(*) - E(adsorbent) and bulk choesive energy was calculated as: E_{coh} = [E(*adsorbent) - E(*) -n$E_{Ru,g}$]/n.

E(*adsorbent), E(*) and E(adsorbent) represent the total energy of * adsorbent, * and adsorbent molecule, respectively. $E_{Ru,g}$ is the total energy of an individual Ru atom, n is the number of atoms in the cluster. The Gibbs free energy for each elementary step was calculated as: G = E_{elec} + E_{ZPE} – TS, in which E_{elec} is the electronic energy at 0 K calculated by DFT, E_{ZPE} is the zero-point energy term, and T is the absolute temperature (here 298.15 K).

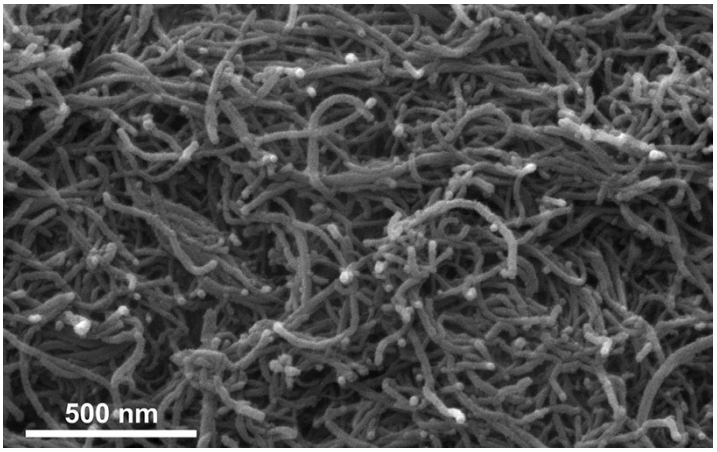

Fig. S1 SEM image of Ru/B-CNT.

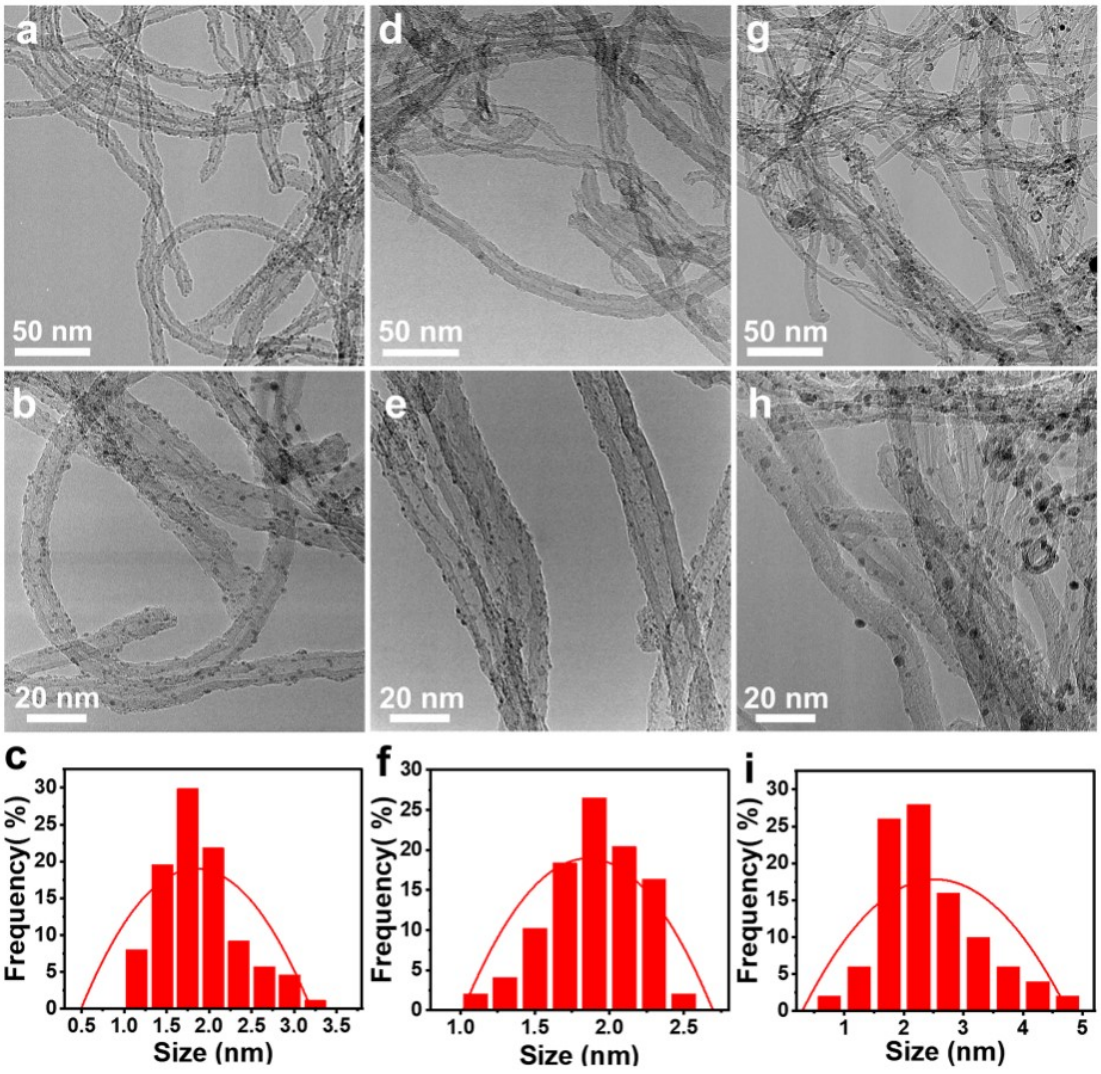

Fig. S2 The HRTEM images and the size distributions of (a, b, c) Ru/B-CNT, (d, e, f) B-Ru/CNT, (f, g, i) Ru/CNT.

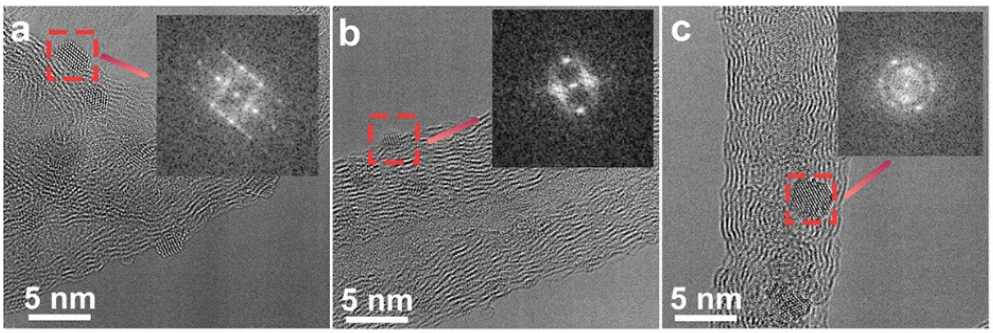

Fig. S3 The HRTEM images, inset: the corresponding fast Fourier transform pattern. (a) Ru/B-CNT, (b) B-Ru/CNT, (c) Ru/CNT.

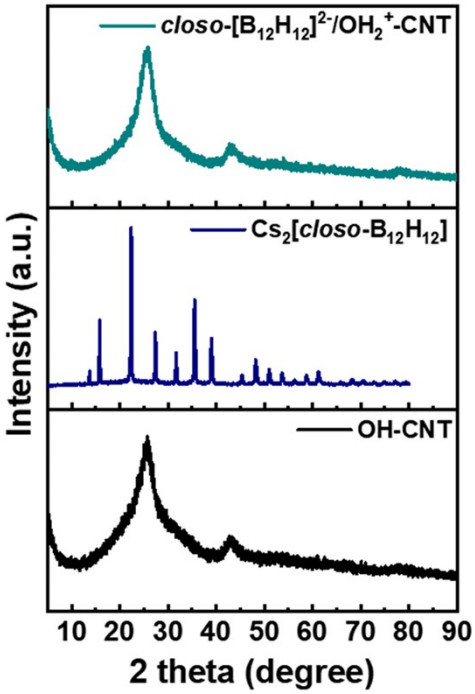

Fig. S4 XRD patterns of OH-CNT, Cs_2[*closo*-$B_{12}H_{12}$], *closo*-$[B_{12}H_{12}]^{2-}$/OH_2^+-CNT.

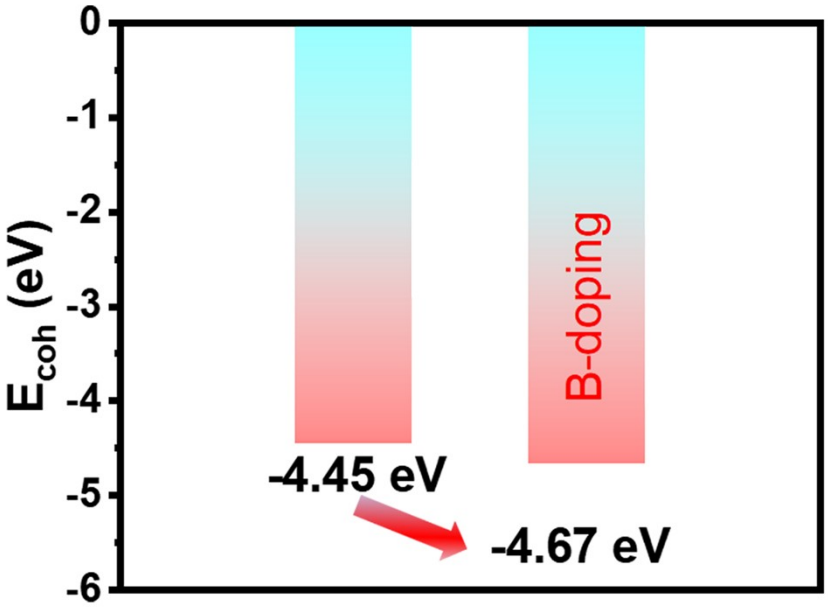

Fig. S5 The calculated bulk cohesive energy (E_{coh}) of Ru NPs before and after B doping.

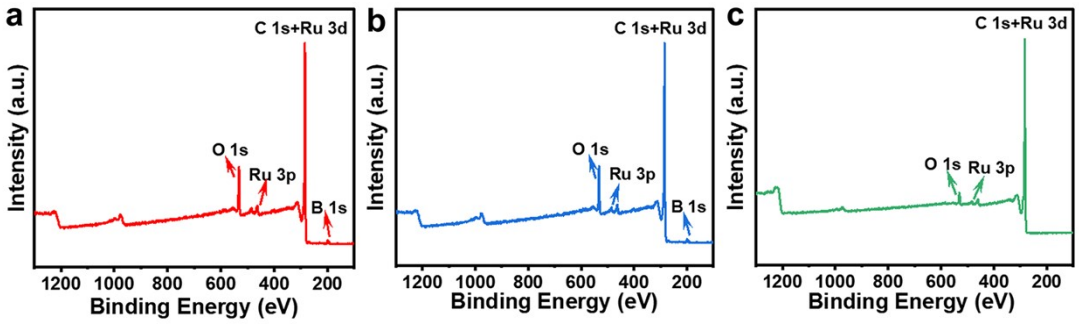

Fig. S6 XPS survey spectrum data, (a) Ru/B-CNT, (b) B-Ru/CNT, (c) Ru/CNT.

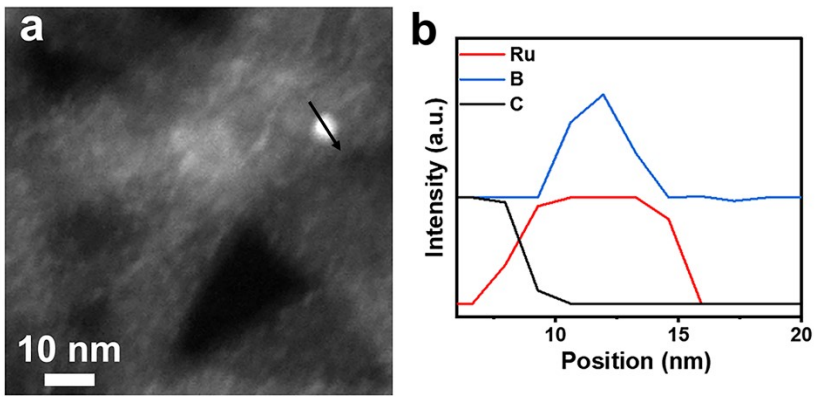

Fig. S7 (a) HAADF-STEM image of Ru/B-CNT. (b) Line-profile analysis from the indicated area of (a).

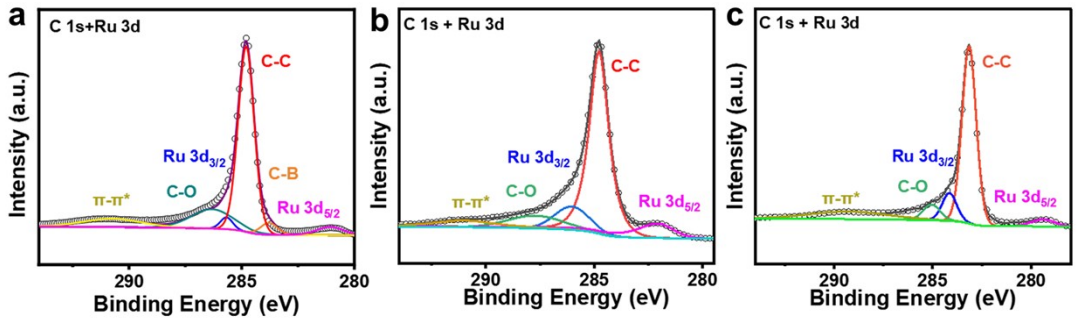

Fig. S8 High resolution XPS spectra data of C 1s, (a) Ru/B-CNT, (b) B-Ru/CNT, (c) Ru/CNT.

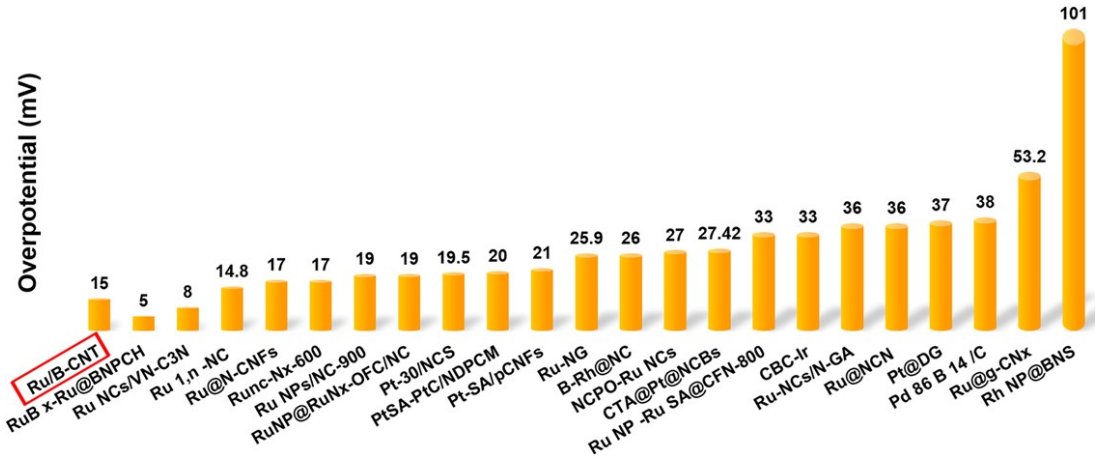

Fig. S9 HER activity comparison between Ru/B-CNT and reported state-of-art ruthenium metal-based catalysts and other noble group metal-based catalysts in 1 M KOH.

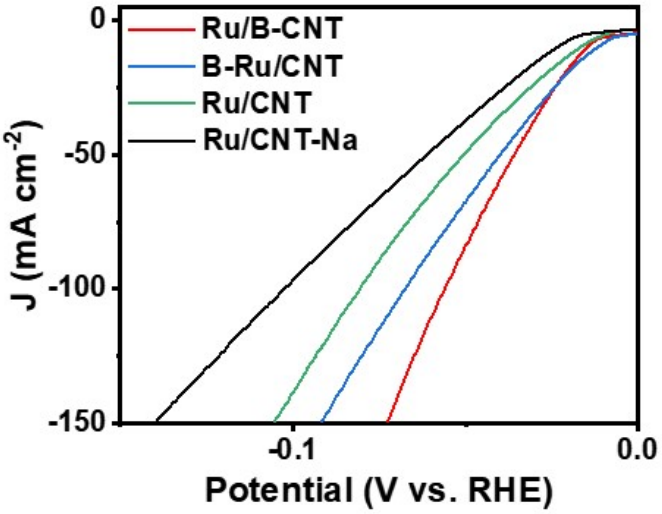

Fig. S10 The comparison of electrocatalytic HER performance of Ru/B-CNT, B-Ru/CNT, Ru/CNT and Ru/CNT-Na in alkaline solution.

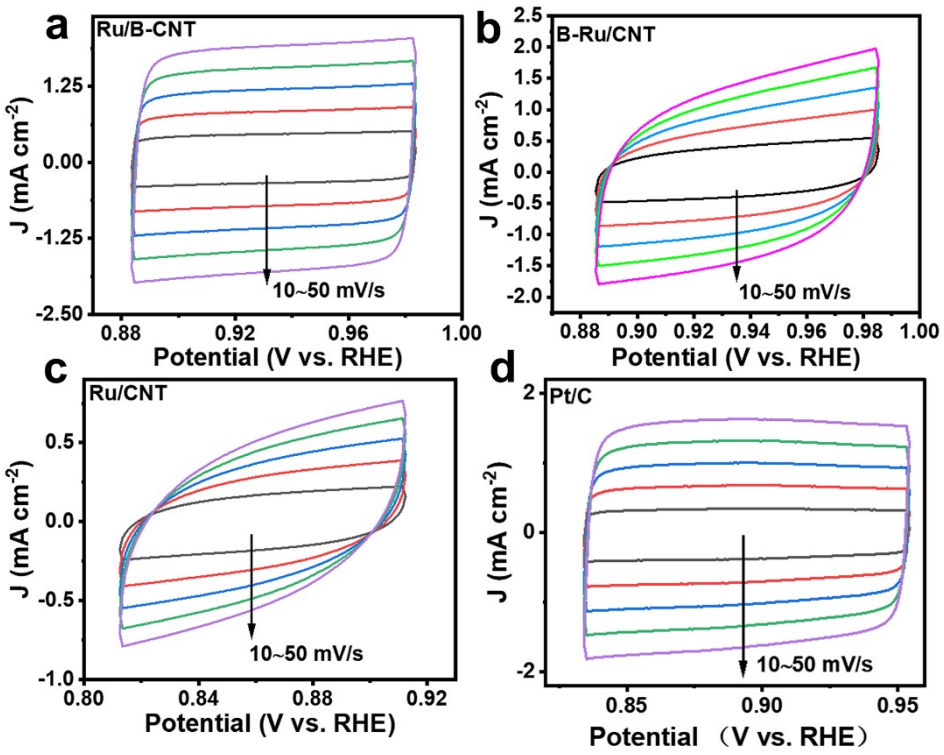

Fig. S11 CV measurements in a non-faradic current region at scan rates of 10, 20, 30, 40, 50 mV s^{-1} of (a) Ru/B-CNT, (b) B-Ru/CNT, (c) Ru/CNT.

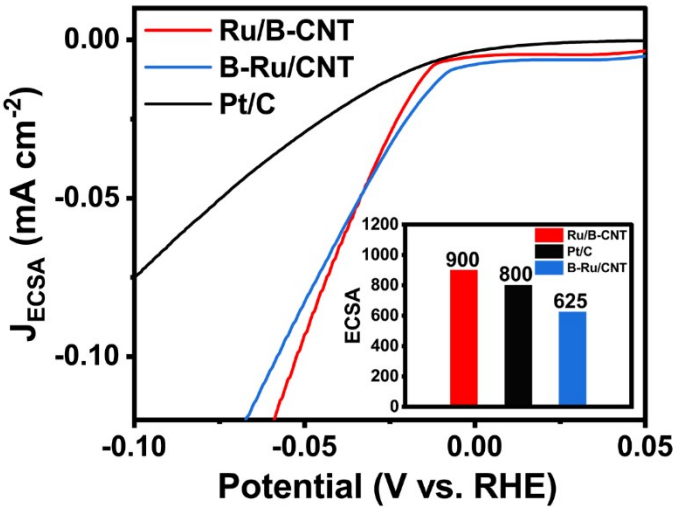

Fig. S12 The ECSA-normalized LSV curves of catalysts Ru/B-CNT, B-Ru/CNT, Ru/CNT and Pt/C. The inset is the ECSA of catalysts.

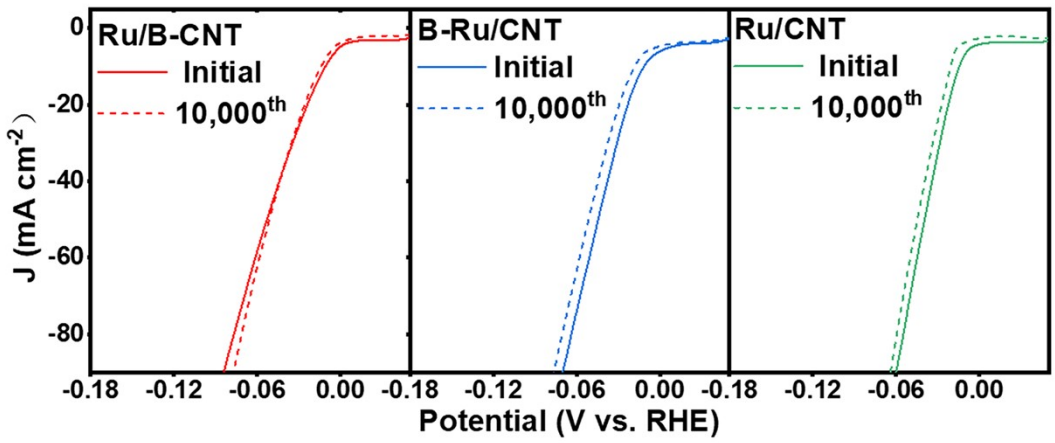

Fig. S13 The polarization curves of Ru/B-CNT, and B-Ru/CNT, and Ru/CNT before and after 10,000 cycles in 1 M KOH solution.

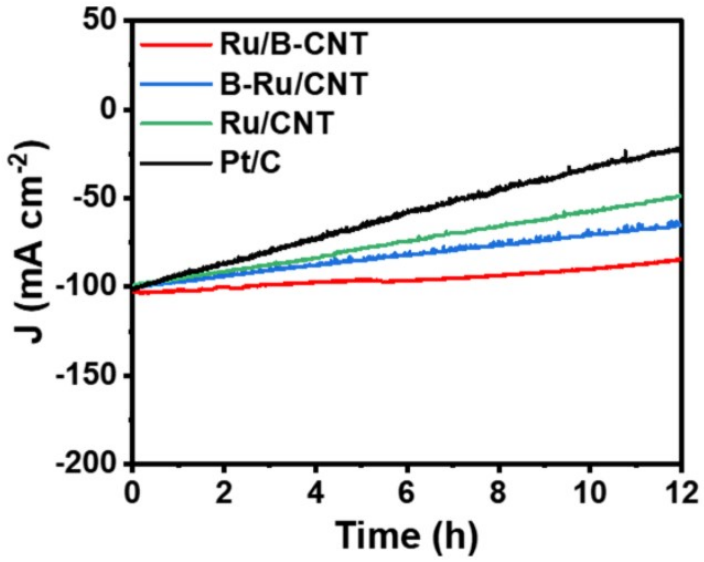

Fig. S14 Chronoamperometric curves operated at a fixed voltage corresponding to 100 mA cm^{-2}.

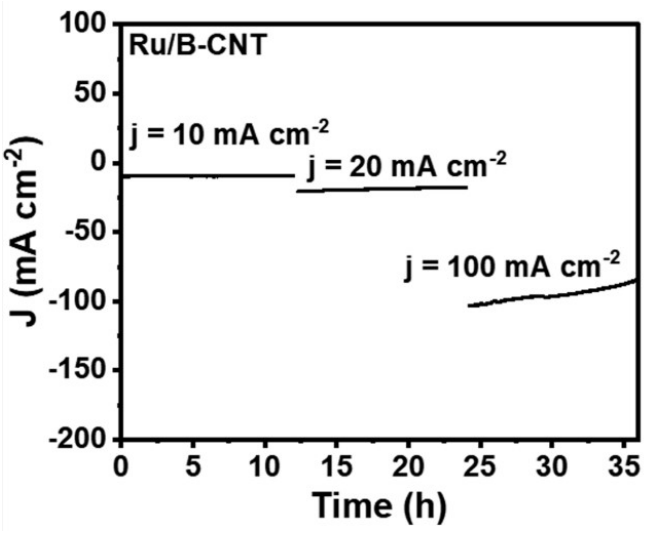

Fig. S15 Chronoamperometric curve operated at fixed potentials corresponding to current densities 10, 20 and 100 mA cm^{-2}.

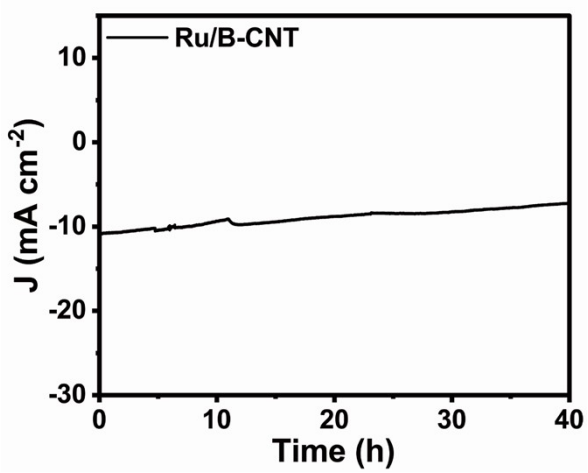

Fig. S16 Chronoamperometric curve operated at fixed potentials corresponding to current densities 10 mA cm^{-2} for 40h.

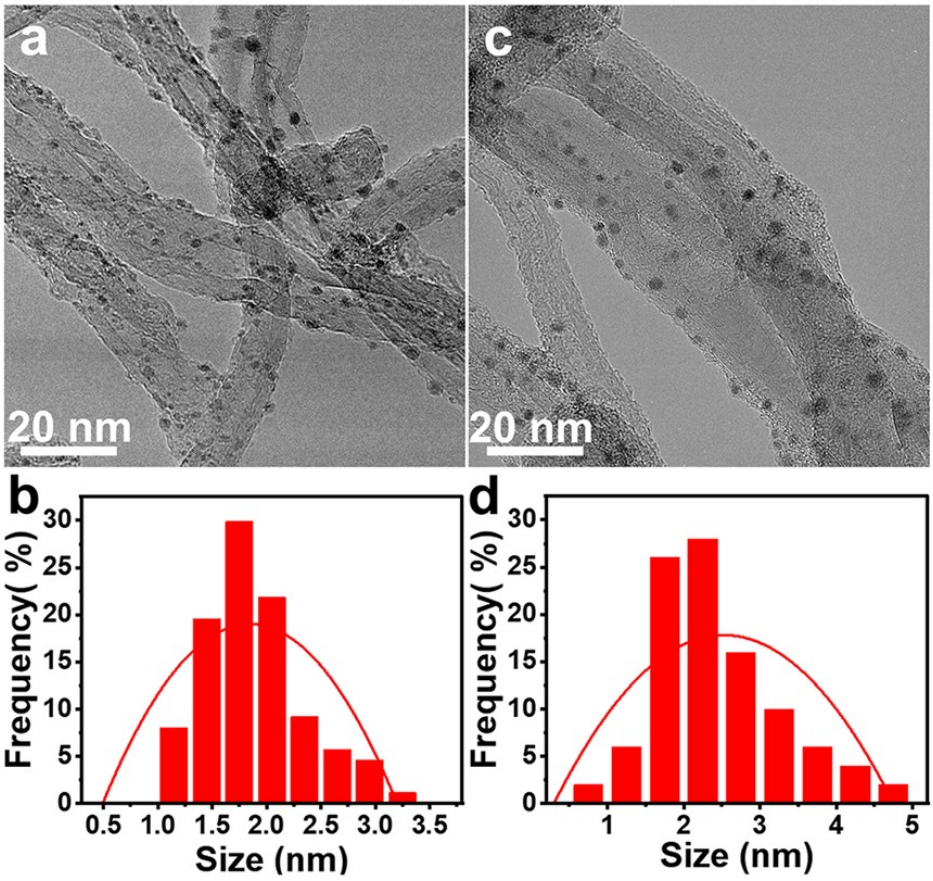

Fig. S17 TEM images and the size distributions of (a, b) before chronoamperometry test, (c, d) after chronoamperometry test.

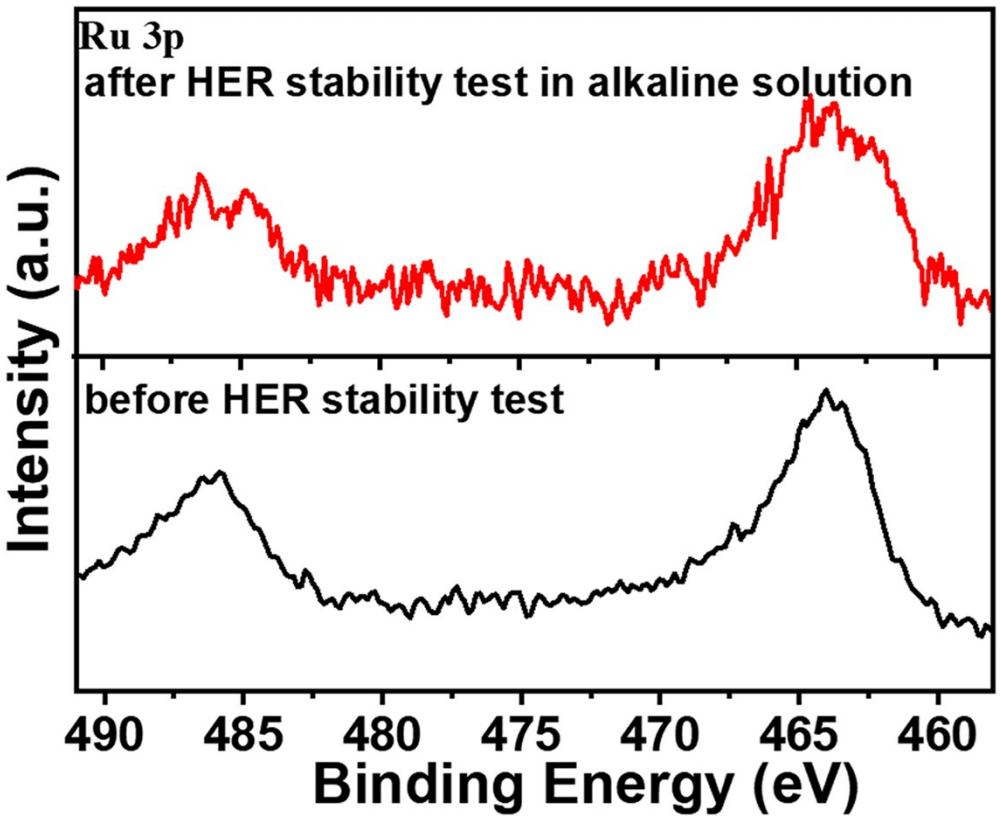

Fig. S18 High resolution XPS data of Ru 3p of Ru/B-CNT before and after 24h of chronoamperometry test in 1 M KOH.

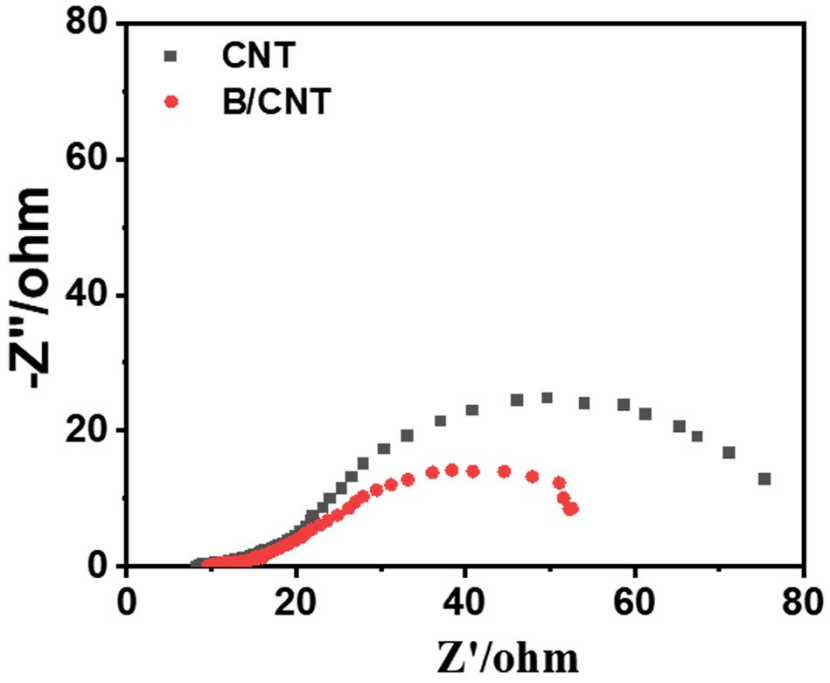

Fig. S19 Electrochemical impedance spectra of CNT and B/CNT.

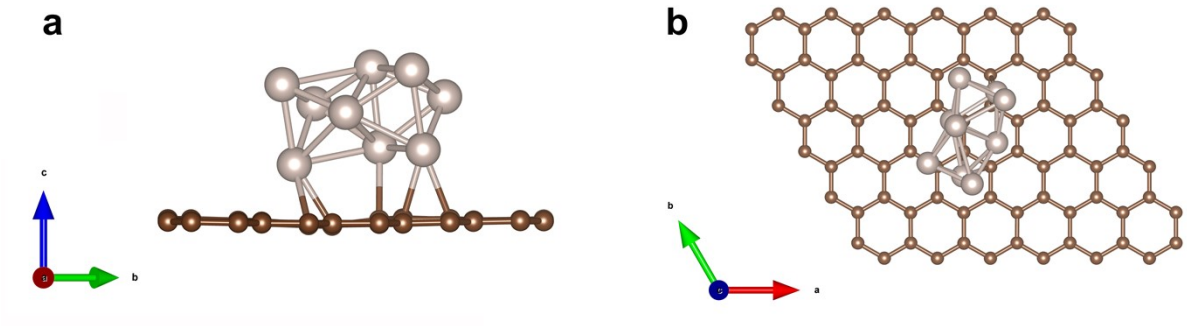

Fig. S20 The structure models of Ru/CNT (a) side view and (b) top view used in DFT calculations. The gray and brown balls represent Ru and C, respectively.

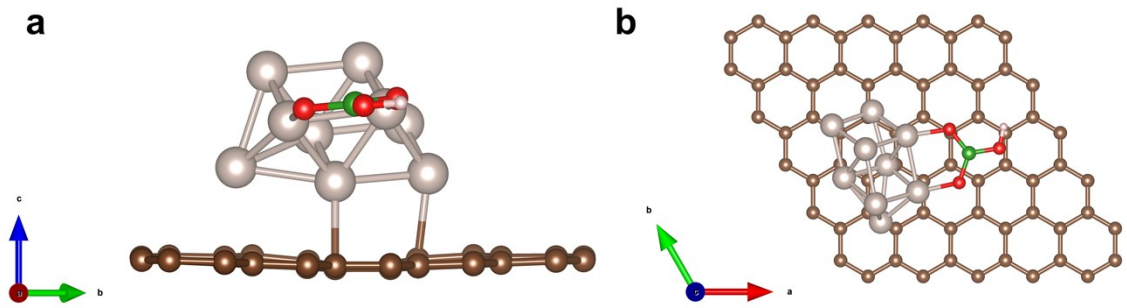

Fig. S21 The structure models of B-Ru/CNT (a) side view and (b) top view used in DFT calculations. The gray balls, brown balls, green balls and red balls represent Ru, C, B and O, respectively.

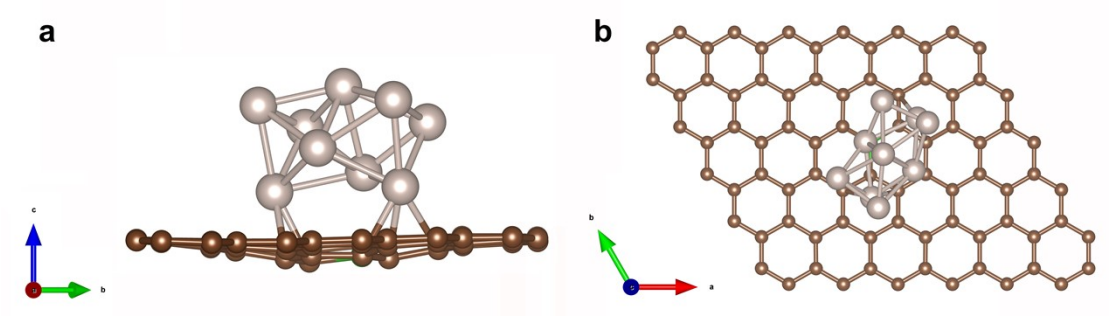

Fig. S22 The structure models of Ru/B-CNT (a) side view and (b) top view used in DFT calculations. The gray balls, brown balls, and green balls represent Ru, C, and B, respectively.

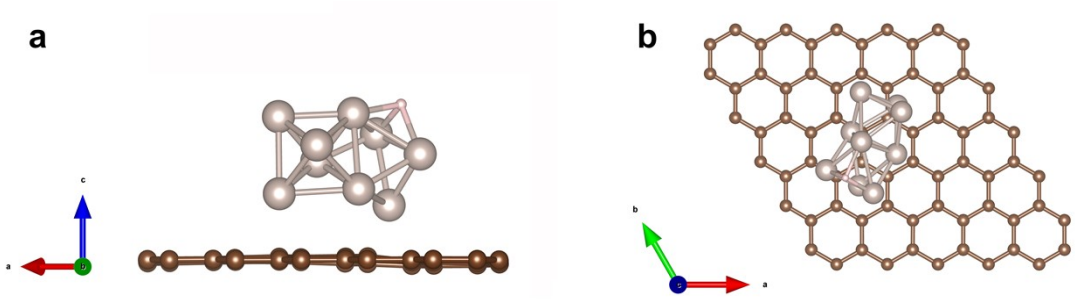

Fig. S23 The optimized structure models of the adopted adsorption H sites on Ru of Ru/CNT (a) side view and (b) top view. The gray, light pink and brown balls represent Ru, H and C, respectively.

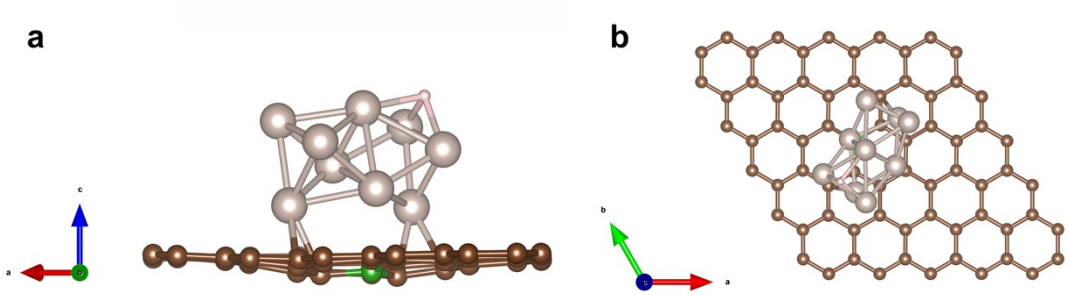

Fig. S24 The optimized structure models of the adopted adsorption H sites on Ru of Ru/B-CNT (a) side view and (b) top view. The gray, light pink, green balls and brown balls represent Ru, H, B and C, respectively.

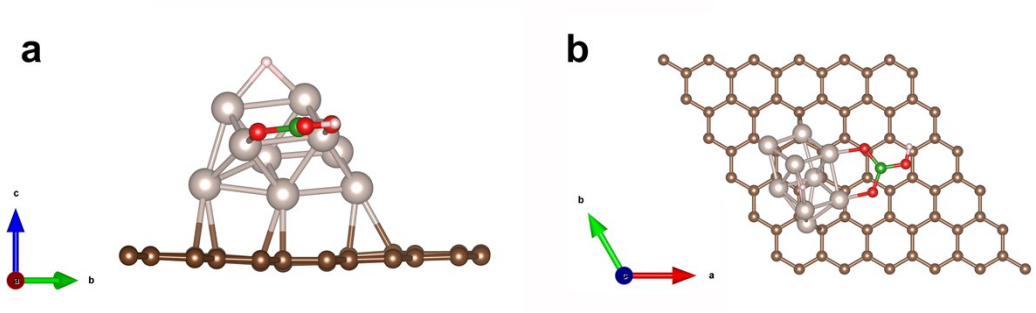

Fig. S25 The optimized structure models of the adopted adsorption H sites on Ru (far B) of B-Ru/CNT (a) side view and (b) top view. The gray, light pink, green balls, red balls and brown balls represent Ru, H, B, O and C, respectively.

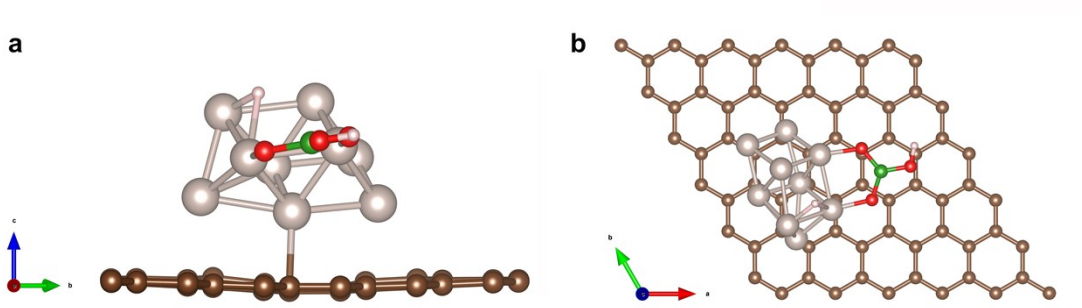

Fig. S26 The optimized structure models of the adopted adsorption H sites on Ru (near B) of B-Ru/CNT (a) side view and (b) top view. The gray, light pink, green balls, red balls and brown balls represent Ru, H, B, O and C, respectively.

Table 1 The resistance parameters obtained from Randles equivalent circuit fitting.

Sample	R_s (Ω)	R_{ct} (Ω)
Ru/B-CNT	8.5	13.5
B-Ru/CNT	8.6	15.7
Ru/CNT	9.0	36.0
Pt/C	11.4	54.1

References

1 G. Kresse, J. Furthmüller, *Comput. Mater. Sci.*, 1996, **6**, 15-50.

2 G. Kresse, J. Furthmüller, *Phys. Rev. B*, 1996, **54**, 11169-11186.

3 J. P. Perdew, K. Burke, M. Ernzerhof, *Phys. Rev. Lett.*, 1996, **77**, 3865-3868.

4 G. Kresse, D. Joubert, *Phys. Rev. B*, 1999, **59**, 1758-1775.

5 P. E. Blöchl, *Phys. Rev. B*, 1994, **50**, 17953-17979.

6 H. J. Monkhorst, J. D. Pack, *Phys. Rev. B*, 1976, **13**, 5188-5192.

7 S. Grimme, J. Antony, S. Ehrlich, H. Krieg, *J. Chem. Phys.*, 2010, **132**, 154104.

8 S. Grimme, S. Ehrlich, L. Goerigk, *J. Comput. Chem.*, 2011, **32**, 1456-65.

9 J. Tang, B. Wang, Y. Zhang, X. Zhang, Q. Shen, J. Qin, S. Xue, X. Guo, C. Du, J. Chen, *J. Mater. Chem. A*, 2022, **10**, 4181-4190.

10 J. Zhao, H. Guo, Y. Li, L. Zheng, H. Ren, L. Zhao, R. Song, *J. Mater. Chem. A*, 2023, **11**, 18375-18386.

11 Q. He, Y. Zhou, H. Shou, X. Wang, P. Zhang, W. Xu, S. Qiao, C. Wu, H. Liu, D. Liu, S. Chen, R. Long, Z. Qi, X. Wu, L. Song, *Adv. Mater.*, 2022, **34**, 2110604.

12 G. Zhou, S. Zhang, Y. Zhu, J. Li, K. Sun, H. Pang, M. Zhang, Y. Tang, L. Xu, *Small*, 2023, **19**, 2206781.

13 Z. Wu, L. Liu, Z. Zhao, C. Yang, S. Mu, H. Zhou, X. Luo, T. Ma, S. Li, C. Zhao, *Small*, 2023, **19**, 2204738.

14 Y. Feng, W. Feng, J. Wan, J. Chen, H. Wang, S. Li, T. Luo, Y. Hu, C. Yuan, L. Cao, L. Feng, J. Li, R. Wen, J. Huang, *Appl. Catal., B*, 2022, **307**, 121193.

15 Z. Jiang, S. Song, X. Zheng, X. Liang, Z. Li, H. Gu, Z. Li, Y. Wang, S. Liu, W. Chen, D. Wang, Y. Li, *J. Am. Chem. Soc.*, 2022, **144**, 19619-19626.

16 W. Yang, M. Li, B. Zhang, Y. Liu, J. Zi, H. Xiao, X. Liu, J. Lin, H. Zhang, J. Chen, Z. Wan, Z. Li, G. Li, H. Li, Z. Lian, *Adv. Funct. Mater.*, 2023, 2304852.

17 Q. Liang, Q. Li, L. Xie, H. Zeng, S. Zhou, Y. Huang, M. Yan, X. Zhang, T. Liu, J. Zeng, K. Liang, O. Terasaki, D. Zhao, L. Jiang, B. Kong, *ACS Nano*, 2022, **16**, 7993-8004.

18 T. Luo, J. Huang, Y. Hu, C. Yuan, J. Chen, L. Cao, K. Kajiyoshi, Y. Liu, Y. Zhao, Z. Li, Y. Feng, *Adv. Funct. Mater.*, 2023, **33**, 2213058.

19 Y. Han, H. Duan, W. Liu, C. Zhou, B. Wang, Q. Jiang, S. Feng, W. Yan, T. Tan, R. Zhang, *Appl. Catal., B*, 2023, **335**, 122898.

20 Q. Yang, H. Liu, P. Yuan, Y. Jia, L. Zhuang, H. Zhang, X. Yan, G. Liu, Y. Zhao, J. Liu, S. Wei, L. Song, Q. Wu, B. Ge, L. Zhang, K. Wang, X. Wang, C. R. Chang, X. Yao, *J. Am. Chem. Soc.*, 2022, **144**, 2171-2178.

21 Q. Yu, Y. Fu, J. Zhao, B. Li, X. Wang, X. Liu, L. Wang, *Appl. Catal., B*, 2023, **324**, 122297.

22 Y. Li, Y. Luo, Z. Zhang, Q. Yu, C. Li, Q. Zhang, Z. Zheng, H. Liu, B. Liu, S. Dou, *Carbon*, 2021, **183**, 362-367.

23 X. Xiao, H. Zhang, Y. Xiong, F. Liang, Y. W. Yang, *Adv. Funct. Mater.*, 2021, **31**, 2105562.

24 J. Li, J. Liu, C. Chen, J. Guo, R. Bi, S. Chen, L. Zhang, M. Zhu, *Chem. Eng. J.*, 2022, **436**, 135186.

25 X. Chen, X. An, L. Tang, T. Chen, G. Zhang, *Chem. Eng. J.*, 2022, **429**, 132259.

26 B. Sarkar, D. Das, K. K. Nanda, *J. Mater. Chem. A*, 2021, **9**, 13958-13966.

27 Y. Ding, K. W. Cao, J. W. He, F. M. Li, H. Huang, P. Chen, Y. Chen, *Chinese. J. Catal.*, 2022, **43**, 1535-1543.

28 T. Jiang, L. Yu, Z. Zhao, W. Wu, Z. Wang, N. Cheng, *Chem. Eng. J.*, 2022, **433**, 133525.

29 K. Chen, Z. Wang, L. Wang, X. Wu, B. Hu, Z. Liu, M. Wu, *Nano-Micro Lett*, 2021, **13**, 138.